Journal of Materials Chemistry B

Accepted Manuscript

ROYAL SOCIETY OF CHEMISTRY

www.rsc.org/materialsB

Reactive Oxygen Species (ROS) Responsive PEG-PCL Nanoparticles with pH-Controlled Negative-to-Positive Charge Reversal for Intracellular Delivery of Doxorubicin

Hongzhang Deng[a, c], Xuefei Zhao[a, c], Jinjian Liu[b], Liandong Deng[a], Jianhua Zhang[a], Jianfeng Liu[b], Anjie Dong[a,c]*

[a] Department of Polymer Science and Technology School of Chemical Engineering and Technology , Tianjin University, Tianjin 300072, P.R. China
[b] Tianjin Key Laboratory of Padiation Molecular and Molecular Nuclear Medicine, Institute of Radiation Medicine, Chinese Academy of Medical Science and Peking Union Medical College, Tianjin, 300192, P.R.China
[c] Collaborative Innovation Center of Chemical Science and Engineering (Tianjin), Tianjin 300072, P.R. China
*Corresponding Author ajdong@tju.edu.cn

Nanocarriers have been extensively explored for cancer drug delivery with their ability to respond to cancer heterogeneity which is recently recognized as a critical door way to a high therapeutic index. We proposed to develop a polycaprolactone bearing acid-labile β-carboxylic amides segments with charge reversal property, which was coupled to mPEG with thioether as a linker. The linker could respond to overproduced reactive oxygen species (ROS) of cancer cells (ROS, e.g., perhaps more than one order of magnitude higher than healthy cells). This tailor-made surface charged nanoparticles (NPs) exhibited a capacity of reversing its surface charge from negative to positive at tumor extracellular environment (pH ~ 6.8) for enhancing cell internalization and an ability of response to the tumor ROS heterogeneity at the tumor intracellular environment to accelerate the release of drug from NPs. The *in vitro* release studies showed that DOX release was greatly accelerated under the intracellular prevailing ROS (hydrogen peroxide (H_2O_2) simulating the oxidative stress). Cell uptake showed that the NPs could be more effectively internalized at pH 6.8 (simulating tumor extracellular condition) than at pH 7.4. The MTT assay demonstrated that the DOX loaded NPs showed significant cytotoxicity to HepG2 cancer cells while no influence on the L02 normall cells. These ROS sensitive and surface charged NPs with superior cell internalization ability and rapid intracellular drug release provided a novel platform for tumor-targeting drug delivery.

Introduction

Nanocarriers fabricated from amphiphilic copolymers have been extensively explored for cancer drug delivery to increase the solubility of the drug in water and tumor accumulation by mean of its enhanced permeation and retention effect.[1-5] However, one practical challenge of nanoparticles (NPs) was their poor cellular uptake and the unsatisfactory intracellular drug release which always hampered the efficacy of cancer chemotherapy.[6-11] To overcome these limitations, environment-responsive nanocarriers have been attempted to improve the drug bioavailability.[12-15] Their ability of responding to cancer heterogeneity was recently recognized as a critical doorway to a high therapeutic index.[16-19] Cancer cells were reported to overproduce reactive oxygen species (ROS) and thus under increased oxidative stress.[20-22] These cells may exist in different tumors, but may also coexist in different regions in one tumor, and even one tumor cell at different stages may have different ROS levels. ROS heterogeneity sensitivity is one of the promising internal stimuli interesting for biomedical applications, due to the existence of a high ROS difference between the mildly oxidizing extracellular space and the reducing intracellular space.[21, 23] So the intracellular drug release could be enhanced using ROS bio-responsive biodegradable NPs. Thioethers have a characteristic of ROS response due to the changes from hydrophobic to hydrophilic under ROS environment then triggering hydrolysis of phenol ester linked with thioether.[24]

However, those responsive delivery systems only utilize ROS-triggered drug release acceleration at the tumor cells, and the enhancement of the cell internalization was rarely involved.[25-28] Cellular uptake is directly related to the interactions between NPs and biological environment which depends on the physicochemical properties of surface charge.[29-32] Neutral and negatively charged NPs were adsorbed less on cell membranes and consequently exhibited lower internalization extent comparing to positively charged NPs.[33-37] But the positively charged NPs showed strong interaction with bovine serum albumin protein which caused severe aggregation and rapidly clearance from circulation.[35, 38-40] In order to balance this contradiction, pH-dependent charge conversion which was triggered by the unique tumor extracellular pH (extracellular environment pH 6.5 - 7.2, physiological conditions pH 7.4) has been proved to be a very efficient strategy for the improved drug delivery.[41-43] Kataoka reported some smart carriers that were negatively charged under physiological conditions and positively charged at endosomal pH values.[44-47] Wang Jun reported a tumor-acidity activated charge-conversional nanogel that could be transformed from a negatively charged form into a positively charged form. The conversion enhanced the cellular uptake of the nanogel and promoted the cargo release, which led to remarkably enhanced efficiency in killing cancer cells.[47] These studies have

demonstrated the feasibility of the tumoral extracellular acidity activated charge-reversal strategy. Those charge-reversal delivery systems which were only response to the extracellular pH condition cannot efficiently release the drug from carriers in intracellular environment. Furthermore, most of the charge-conversional nanomedicines studied previously were limited to using β-carboxylic acid groups to reversibly mask the primary and secondary amine groups of cationic polymers, such as poly(ethylene imine) and polylysine. Unfortunately, the in vivo applications of these polycations were greatly limited due to their high cytotoxicity to cells.[49] As one of the most widely used biopolymers for drug delivery, PEG-b-PCL has excellent biocompatibility. However, to the best of our knowledge, very few studies have been carried out to introduce a pH-sensitive charge-conversion function to PEG-b-PCL NPs.[50, 51, 52]

In this paper, we reported a novel design and preparation of degradable NPs based on ROS sensitive thioether-linked PEG-b-PCL containing pH-sensitive charge-conversional pendants to enhance cell uptake. As shown in **Scheme 1**, the acid-labile β-carboxylic amides in the block copolymers provided the pH-dependent charge-conversional feature to the NPs which resulted in the transform surface charge of the NPs depending on the environment acidity. Meantime ROS sensitive linkers of those NPs preferentially degraded at ROS heterogeneity of cancer cells leading to an efficiency intracellular drug release. Here, the charge-reversal and ROS sensitive NPs were prepared and the charge-reversal behavior of the NPs, DOX loading, ROS-responsive release of DOX, as well as anti-tumor activity of DOX-loaded NPs were investigated.

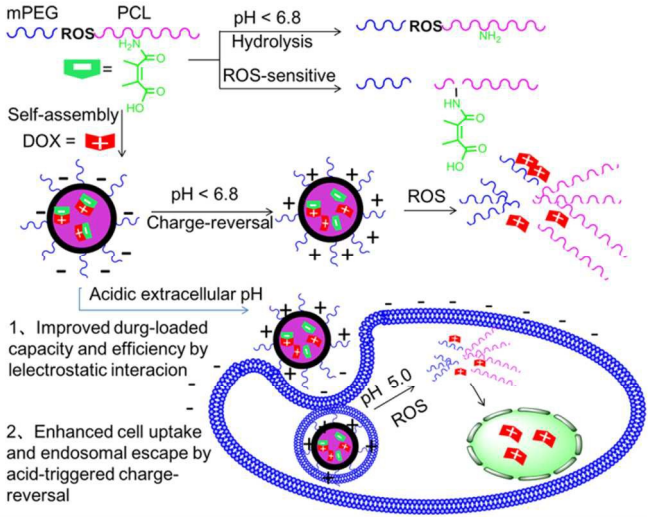

Scheme 1 Illustration of charge-conversional behavior and ROS-sensitivity of mPEG-ros-P(CL-co-DCL) NPs for active loading and triggered release of DOX by intracellular ROS.

Experimental

Materials

γ-(carbamic acid tert-butyl ester)-ε-caprolactone (CATCL) and mPEG-MAA-EDT-MAA were synthesized according to a previous method and detail information was given in supporting information[49, 53]. Methoxy poly (ethylene glycol) (mPEG, Mn=5.0×10^3g/mol), stannous octoate ($Sn(Oct)_2$), ε-caprolactone (ε-CL), and phenylcarbinol were used as received from Sigma-Aldrich (Milwaukee, USA). Methacryloyl chloride, trifluoroacetic acid (TFA), p-hydroxy benzaldehyde (Hy), phenylcarbinol (PA), 2-aminoethanethiol hydrochloride, 2,3-Dimethylmaleic anhydride (DMMA) and 1,2-Ethanedithiol (EDT) were purchased from GL Biochem (Shanghai) Ltd. Tetrahydrofuran (THF) and triethylamine were dried by refluxing over Na metal under an argon atmosphere and distilled immediately before use. Dichloromethane (DCM) was purified by vacuum distillation with CaH_2. 3-(4,5-Dimethylthiazol-2-yl)-2,5-diphenyltetrazolium bromide (MTT) was purchased from Sigma-Aldrich. Doxorubicin hydrochloride (DOX·HCl) was purchased from Wuhan Hezhong Biochemical in manufacturing co.,Ltd.

Dulbecco's modified Eagle's medium (DMEM), Opti-MEM and bovine serum (FBS) were purchased from Invitrogen Corporation (Carlsbad, CA). Dimethyl sulfoxide (DMSO) was purchased from Sigma-Aldrich.

HepG2 and L02 cells were purchased from American Type Culture Collection (ATCC; Manassas, VA). Cell culture medium and fetal bovine serum were from WisentInc (Multicell, WisentInc., St. Bruno, Quebec, Canada). HepG2 and L02 cells were maintained in Dulbecco's Modified Eagle's Medium (DMEM) with 10% fetal bovine serum and 1% antibiotic solution. All cells were cultured in a humidified atmosphere containing 5 % CO_2 at 37 ºC.

Measurments

^{1}H-NMR spectra were recorded on a Varian Inova 500 spectrometer operating at 500 MHz (Varian Inc., Palo Alto, USA) using $CDCl_3$ as a solvent and tetramethylsilane (TMS) as the internal standard. The number-average molecular weight (M_n) and polydispersity index (M_w/M_n) of copolymers were determined by gel permeation chromatography (GPC) using a Malvern Viscotek GPC max system which was equipped with a porous styrene divinylbenzene copolymer-based column (CLM3009, T6000M, General Mixed, Org 300 × 7.8 mm). THF was used as the eluting solvent with a flow rate of 1 mL/min and polystyrene

was used as standard for calibration. The size and size distribution (PDI) of NPs were performed using a laser particle size analyzer (zetasizer Nano, Malvern, UK) at a wavelength of 633 nm with a constant angle of 173 °C. The diameter of NPs was received from the average of three measurement results. Morphologies of NPs were observed under a Hitachi H600 transmission electron microscopy (TEM) system at an operated voltage of 75 kV. For TEM measurement, the sample was prepared by adding a drop of NPs solution onto the copper grid, and then the sample was air-dried and measured at room temperature. MALDI-TOF MS was prepared by saturating α-Cyano-4-hydroxycinnamic acid (CHCA) in solution contains 50% (v/v) acetonitrile. A 5 µl aliquot of 0.5 mg/ml sample was mixed with 20 µl of matrix, 1 µl solution was plated onto a 96 spot target plate. MALDI-TOF MS spectra were acquired on a Microflex LT system (Bruker Corporation, Billerica, MA) with 50% laser intensity using standard LP (linear positive) provided by the software.

Synthesis of mPEG-MAA-EDT-MAA-Hy

The mPEG-MAA-EDT-MAA-Hy was prepared via esterification reaction of mPEG-MAA-EDT-MAA with Hy in the presence of DCC/DMAP. Typically, to a solution of mPEG-MAA-EDT-MAA (0.3 g, 0.06 mmol) in 10 mL of dried DCM was added p-hydroxy benzaldenyde (0.07 g, 0.6 mmol), DCC (0.12 g, 0.6 mmol) and DMAP (0.0054 g, 0.02 mmol). The solution was kept at room temperature under stirring for 24 h. The resulting mixture was filtered and the filtrate was concentrated by vacuum rotary evaporation then precipitated with excess diethyl. The product was collected by filtration then dried in vaccumn for 24 h at room temperature. Yield: 93 %.

Synthesis of mPEG-MAA-EDT-MAA-Hy-Cys

In a typical example, under a nitrogen atmosphere, a stirred solution of mPEG-MAA-EDT-MAA-Hy (0.3 g, 0.06 mmol) in DMF (25 mL) was added dropwise a solution of cysteamine hydrochloride (0.05 g, 0.06 mmol) in DMF (10 mL). The flask was sealed and placed into an oil bath thermostatted at 30 °C. The reaction mixture was stirred for 8 h in the dark. The resulting product was dialyzed (M_n = 3500) against water for 24 h and then freeze-dried. Yield: 88 %.

Synthesis of PA-P(CL-co-CATCL)

PA-P(CL-co-CATCL) were synthesized via the ring-opening polymerization of ε-CL and CATCL, respectively using phenylcarbinol as an initiator and $Sn(Oct)_2$ as catalyst. Typically, ε-CL (2.85 g, 25 mmol) and CATCL (2.29 g, 10 mmol) were dissolved in 3 mL of anhydrous toluene in a Schlenk flask at room temperature, followed by three vacuum-nitrogen cycles. Then phenylcarbinol (0.054 g, 0.5 mmol) and $Sn(Oct)_2$ (2.8 mg, 6.94 µmol) was added under nitrogen protection. The reaction mixture was stirred at 140 °C for 12 h and then precipitated with excess diethyl. The resulting white solid was purified by precipitating with diethyl ether for three times. The final product was dried under vacuum at room temperature overnight to give a white solid in yield of 82 %.

Synthesis of PA-P(CL-co-CATCL)-MAA

To a DCM solution (20 mL) of PA-P(CL-co-CATCL) (1.0 g 0.096 mmol) and triethylamine (0.051 g, 0.5 mmol), a solution of methacryloyl chloride (0.026 g, 0.25 mmol) in 10 mL DCM was added dropwise at 0 °C. After completion of addition, the reaction mixture was warmed to room temperature and the reaction proceeded for another 20 h. The resulting polymer PA-P(CL-co-CATCL)-MAA was isolated by precipitation in cold diethyl ether and dried in vacuum. Yield: 95.3%

Deprotection of PA-P(CL-co-ACL)-MAA

A solution of the protected copolymer PA-P(CL-co-CATCL)-MAA (0.5 g in TFA) was placed into a round-bottomed flask. Then, the reaction mixture was stirred for 4 h at 25 ° C and subsequently all the solvents were evaporated. The crude product was dissolved in THF and precipitated twice into hexanes followed by filtration. The residual solvent was removed under vacuum to obtain the deprotected copolymer PA-P(CL-co-ACL)-MAA bearing γ-amino groups. Yield : 82%.

Synthesis of PA-P(CL-co-(DMMA-CL))-MAA (PA-P(CL-co-DCL)-MAA)

PA-P(CL-co-ACL)-MAA was dispersed in distilled water and the solution pH was adjusted to 8.5 using 0.1 N NaOH solution. DMMA was added into the solution and the pH was maintained at 8.5 by adding 0.1 N NaOH. The mixture was stirred for 3 h at room temperature and then dialyzed against distilled water followed by lyophilization.

Synthesis of and mPEG-ros-P(CL-co-DCL)

mPEG-MAA-EDT-MAA-Hy-Cys (0.20 g, 0.038 mmol) and PA-P(CL-co-ACL-co-(DMMA-CL))-MAA (0.39 g, 0.038 mmol) were dissolved in 15 mL THF in a 100 mL round-bottom quartz flask, followed by N_2 bubbling with a gentle flow for 30 min to eliminate dissolved oxygen. Then the mixture was stirred at room temperature. After 24 h, the mixture was concentrated by evaporation in vacuo. Residues were poured into large cold diehyl ether three times to cause precipitation and give the final product. Yield: 90 %.

Preparation of mPEG-ros-P(CL-co-DCL) NPs

mPEG-ros-P(CL-co-DCL) NPs were prepared by dialysis method. Typically, 10 mg mPEG-ros-P(CL-co-DCL) polymers was dissolved in dimethylformamide (DMF) and added dropwise to double distilled water. After that, the solution was transferred to a dialysis bag (*M*n = 3500) and dialyzed to remove the organic solvents.

Critical aggregation concentration (CAC) determination

The CAC was measured by a steady state fluorescent-probe methodology using pyrene as probe on a Varian fluorescence spectrophotometer at room temperature. The pyrene-loaded NPs were diluted with the concentration between 10^{-6} and 0.1 mol/L in deionized water. The final pyrene concentration in the copolymer solution was kept at 6×10^{-7} mol/L. The solution was shaken vigorously and then allowed to equilibrate at 25 °C for at least 24 h. The pyrene excitation spectra with different

copolymer concentrations were measured at the detection emission wavelength (λ_{em}=373 nm). The CAC value was evaluated from the intersection of the tangent to the horizontal line of I_{337}/I_{333} with relative constant value and the diagonal line with rapidly increased I_{337}/I_{333} ratio.

Drug loading and release experiments

Typically, mPEG-ros-P(CL-co-DCL) (100 mg) and DOX (15mg) were dissolved in DMF, The mixture solution was dropwise added to double distilled water under magnetic stirring. Then, the mixture was placed in a dialysis bag (*M*n 3500 Da) and free dialyzed against a phosphate buffer (pH 7.4,) to form NPs. The amount of DOX was determined by UV-Vis spectrophotometer. Drug loading content (DLC) and drug loading efficiency (DLE) were calculated from the following equations:

$$\mathrm{DLC}\ (\%) = \frac{\text{weight of loaded drug}}{\text{weight of drug - loaded micelles}} \times 100\% \quad \text{-------}[1]$$

$$\mathrm{DLE}(\%) = \frac{\text{weight of loaded drug}}{\text{weight of drug in feed}} \times 100\% \quad \text{-------}[2]$$

In vitro release profiles of DOX from the polymer NPs were investigated in three conditions at 37 ^{o}C, i.e. (1) phosphate buffered saline (PBS) (10 mM, pH 7.4), (2) PBS (10 mM, pH 7.4) with 10 mM H_2O_2, (3) PBS (10 mM, pH 6.0), (4) PBS (10 mM, pH 6.0) with 10 mM H_2O_2 were sealed in a dialysis tube (M_n = 3500). The amount of released drug in the incubation medium was quantified by UV-Vis spectrophotometer. The cumulative drug release percentage was calculated by the following equation:

$$Er\ (\%) = \frac{V_t \sum_{1}^{n-1} C_i + V_0 C_n}{m_{DOX}} \times 100\% \text{-------}[3]$$

Where m_{DOX} represents the amount of DOX in the NPs, V_0 is the whole volume of the release media (V_0 = 45 mL), V_t is the volume of the replaced media (V_t= 10 mL), and C_n represents the concentration of DOX in the sample.

ROS dependent stability monitored by an optical analyzer turbiscan

The ROS dependent stability assay was performed using an optical analyzer Turbiscan (Formulaction, France). The mPEG-ros-P(CL-co-DCL) NPs (20 mL, 5 mg/mL) were allocated in a cylindrical glass tube and measurements were carried out using a pulsed near infrared LED source at a wavelength of 880 nm. The light which was transmitted (T) and backscattered (BS) through the whole height of sample was recorded. A latex suspension and a silicon oil were used as reference standards and spectroscopic records were computed as percentage with respect to these standards. The variation of the droplet volume fraction (migration) size (coalescence) were observed as both a variation of backscattering (ΔBS) and light transmission (ΔT) profiles. The Turbiscan Stability Index (TSI) is a parameter, which can be used for estimation of the suspension stability. This parameter is a statistical factor and its value is obtained as the sum of all processes taking place in the studied probe. The samples were scanned every 1 hour of 12 hours. The Turbiscan Easysoft Converter software was used for data elaboration. Experiments were carried at the room temperature.

Cell Viability Assays

MTT Assay

The biocompatibility of NPs was assessed with a methyl tetrazolium (MTT) viability assay against HepG2 cells. The cells were plated in a 96-well plate (5×10^3 cells/well) using DMEM medium supplemented with 10 % fetal bovine serum (FBS), 1 % L-glutamine, antibiotics penicillin (100 IU/mL), and streptomycin (100 μg/mL) for 1 day. The medium was aspirated and replaced by 80 μL of fresh medium supplemented with 10 % FBS. A total of 20 μL mPEG-ros-P(CL-co-DCL) NPs in PBS (10 mM, pH 7.4) was added to yield final NPs concentrations. The cells were cultured at 37℃ in an atomosphere containing 5 % CO_2 for one day. The medium was aspirated and replaced by 100 μL fresh medium. A total of 10 μL MTT solution (5 mg/mL) was added. The cells were incubated for another 4 h. The medium was aspirated, the MTT-formazan generated by live cells was dissolved in 200 μL DMSO, and the absorbance at wavelength of 590 nm of each well was measured using a microplate reader. The relative cell viability (%) was determined by comparing the absorbance at 590 nm with control, which contained only culture medium. Data are presented as average ± SD (n=4).

Cell Uptake Studies

Intracellular release of DOX from DOX-loaded mPEG-ros-P(CL-co-DCL) NPs was followed with fluorescence microscope using HepG2 cells. The cells were cultured on microscope slides in a six well plate (5×10^5 cells/well) using RPMI-1640 medium supplemented with 10 % fetal bovine serum (FBS), 1 % L-glutamine, antibiotics penicillin (100 IU/mL), and streptomycin (100 μg/mL) for 1 h. Then the cells were incubated with DOX-loaded NPs or free DOX for 4 h at 37 ^{o}C in a humidified 5 % CO_2-containing atmosphere. The culture medium was removed and the cells were rinsed three times with PBS. Thereafter, the cells were fixed with 4 % formaldehyde for 30 min at room temperature, and the cell nuclei were stained with 4,6-diamidino-2-phenylindole (DAPI). The fluorescence images were obtained using fluorescence microscope.

Statistical Analysis.

All statistical analysis was performed using SPSS 16.5 software. The statistical significance of differences was determined by one-way analysis of variance (ANOVA). All statistical tests were two-sided. The results are shown as mean ± standard deviation.

Results and discussion

Synthesis of mPEG-MAA-EDT-MAA-Hy-Cys

As shown in **scheme 2A**, the mPEG-MAA-EDT-MAA-Hy was synthesized via the esterification reaction of mPEG-MAA-EDT-MAA with Hy in the presence of DCC/DMAP. Then, the copolymer mPEG-MAA-EDT-MAA-Hy-Cys was obtained by the coupling reaction of mPEG-MAA-EDT-MAA-Hy and cysteamine hydrochloride. The structure and composition were well characterized by ^{1}H-NMR and GPC. As shown in **Fig 1A**, a resonance at 8.2-8.4 ppm that appeared in the spectrum was assigned to the phenyl ring protons (**e** and **f**). The esterification efficiency calculated by comparing the integrals of peak at 8.2 ppm with peak at about 3.4 (methoxy protons of PEG) ppm was about 88.5%. As shown in **Fig. 1B**, a resonance at 2.75 ppm that appeared in the spectrum of mPEG-MAA-EDT-MAA-Hy-Cys was assigned to the -CH_2SH protons (i). This suggested the formation of the thiols groups of copolymers.

Furthermore, the concentration of the thiols groups of copolymers was measured using Ellman reagent 5, 5-dithio-bis(2-nitrobenzoci acid).[54, 55] The Ellmans reagent reacts with thiols to form 2-nitro-5-benzoate; the absorbance of this product can be tracked by UV-vis spectroscopy and serves as a measure of the relative concentration of thiols as shown in **Fig. S2**. This test shows that the monomer conversion of Cys was in accordance with the result calculated by ^{1}H-NMR.

Synthesis of PA-P(CL-co-DCL)-MAA

As shown in **Scheme 2B**, ROP of *ε*-caprolactone and γ-(carbamic acid benzyl ester)-ε-caprolactone (CATCL) monomer has been the approach to prepare PA-P(CL-CATCL). As shown in **Fig. S3A**, PA-P(CL-CATCL) prepared in this way displayed the ^{1}H NMR signals of both phenylcarbinol (**Fig. S3A**, a at 7.3 ppm) and P(CL-co-CATCL) (**Fig. S3A**, **e** at 1.37 ppm for CL and **j** at 3.64 ppm for CATCL) blocks. The monomer conversion and number molecular weight (*Mn*) values of copolymers could be calculated by comparing the integrals for the peak of protons in the CH_2 of CL (at about 1.37 ppm) and methoxy protons of CATCL (at about 3.64 ppm) with phenyl protons of phenylcarbinol (at about 7.3 ppm). As shown in **Table 1**, the CL and CATCL repeat units are in line with the feed ratio, indicating living polymerization characteristics to some extent, as was confirmed by GPC results. All these results seem to suggest that the polymerization of CL and CATCL proceeds in a controlled manner to yield well-defined copolymers.

Secondly, through the reaction with methacryloyl chloride, PA-P(CL-CATCL)-MAA was prepared and all characteristic signals could be clearly seen in **Fig. S3B** (n at 5.5 and 6.1 for the -CH_2 in MAA blocks). Thirdly, the deprotection of PA-P(CL-CATCL)-MAA to generate the amino groups was carried out. After being hydrolyzed, the signal at 1.42 ppm decreases.

Then, the reaction of PA-P(CL-ACL)-MAA with DMMA to get PA-P(CL-co-DCL)-MAA was carried out. The signals at 1.8 ppm for the CH_3 could be clearly seen in **Fig. 1C**.

Synthesis of mPEG-ros-P(CL-co-DCL)

As shown in **Scheme 2C**, the mPEG-ros-P(CL-co-DCL) was sythesized via the Michael addition reaction of mPEG-MAA-EDT-MAA-Hy-Cys with PA-P(CL-co-DCL)-MAA. As shown in **Fig. 1D**, mPEG-ros-P(CL-co-DCL) prepared in this way displayed the ^{1}H NMR signals of both PEG (**Fig. 1D**, at 3.6 ppm) and P(CL-co-CATCL) (**Fig. 1D**, **q** at 1.37 ppm for CL and **p** at 3.64 ppm for CL) blocks. As shown in **Fig. S4A**, MALDI-TOF-MS analysis showed that the peak was 15000, indicating that PEG-MAA-EDT-MAA-Hy-Cys had been successfully conjugated with PA-P(CL-co-DCL)-MAA. We also use the GPC to determine the successful preparation of conjugated polymer mPEG-ros-P(CL-co-DCL) by mPEG-MAA-EDT-MAA-Hy and PA-P(PCL-co-DCL)-MAA. As shown in **Fig. S4B**, the molecular weight of mPEG-ros-P(CL-co-DCL) (15100) was similar to the adding of mPEG-MAA-EDT-MAA-Hy (6000) and PA-P(PCL-co-DCL)-MAA (10000) indicating the successful preparation product. Their molecular weight (Mn) and polydispersity index (Mw/Mn) were determined by ^{1}H-NMR and GPC, and summarized in **Table 1.** We chose $mPEG_{113}$-ros-P(CL_{41}-co-DCL_{22}) as a representative sample for further study.

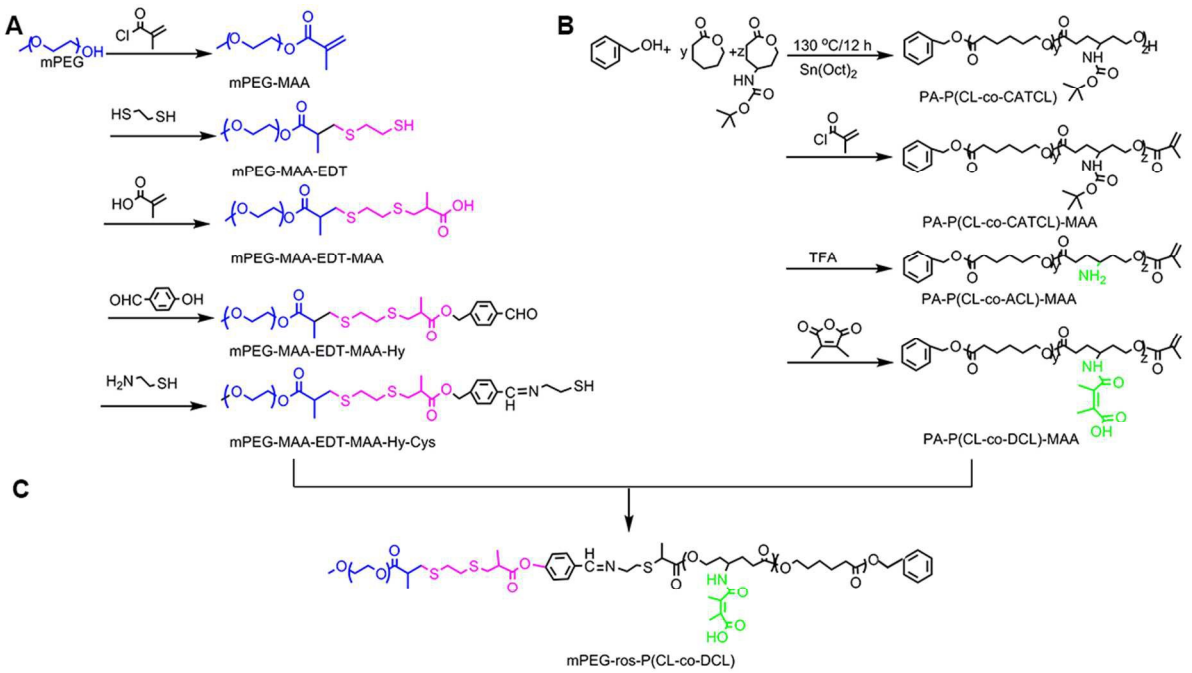

Scheme 2. Synthesis route of mPEG-MAA-EDT-MAA-Hy-Cys (A), synthesis route of PA-P(CL-co-DCL)-MAA (B)**,** synthesis route of mPEG-ros-P(CL-co-DCL) (C).

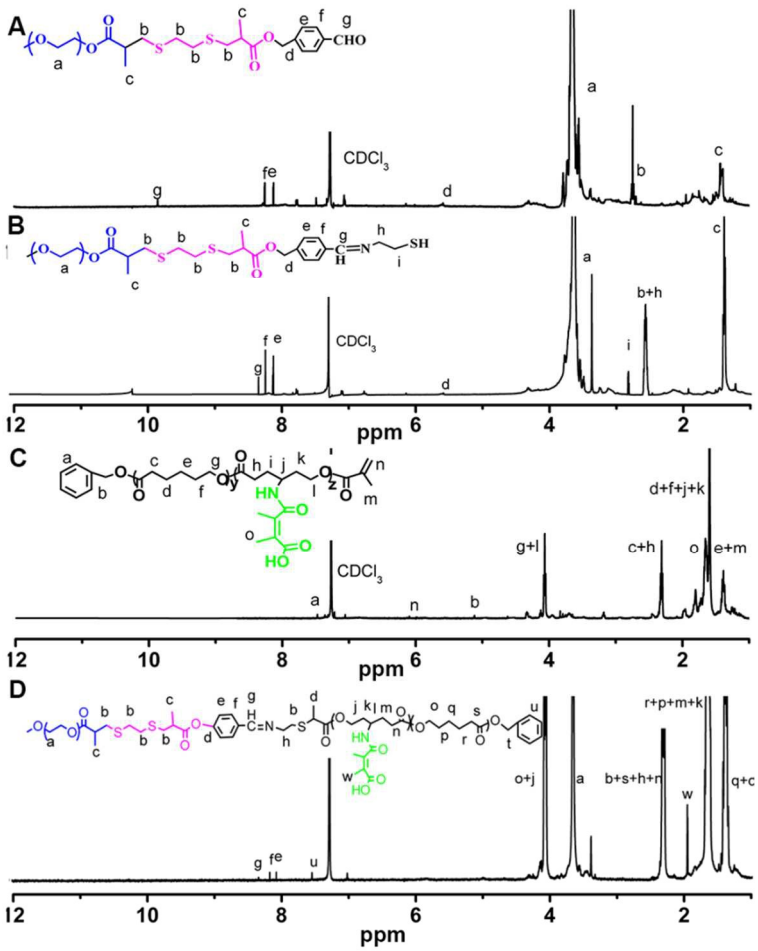

Fig. 1 ^{1}H-NMR characterization of mPEG-MAA-EDT-MAA-Hy (A), mPEG-MAA-EDT-MAA-Hy-Cys (B), PA-b-P(CL-co-DCL) (C) and mPEG-ros-P(CL-co-DCL) (D).

Table 1. Structure and composition of mPEG-ros-P(CL-co-DCL)

Polymers [a]	M_n (g/mol)			M_W/M_n [b]
	Theory	^{1}H-NMR[a]	GPC[b]	
$mPEG_{113}$-ros-P(CL_{42}-co-DCL_{10})	12980	11308	13000	1.2
$mPEG_{113}$-ros-P(CL_{41}-co-DCL_{22})	15260	13018	15100	1.2
$mPEG_{113}$-ros-P(CL_{43}-co-DCL_{33})	16780	14918	16300	1.3

[a] Measured by ^{1}H-NMR

[b] Measured by GPC

Preparation and characterization of mPEG-ros-P(CL-co-DCL) NPs mPEG-ros-P(CL-co-DCL) NPs were prepared by solvent exchange method. As shown in **Fig. 2A**, Laser particle size analyzer measurements showed that mPEG-ros-P(CL-co-DCL) polymers formed monodisperse NPs with low PDI of about 0.2 and sizes of about 100 nm. The morphology of the copolymer NPs was further examined using TEM (**Fig. 2B**) and AFM (**Fig. 2C**). As shown in **Fig. 2**, the NPs were close to spherical and had an average diameter of about 100 nm.

The CAC of mPEG-ros-P(CL-co-DCL) NPs in aqueous solution was characterized using the fluorescence technique with pyrene probe in **Table 2 and Fig. 2D, Fig.2E**. The CAC values of mPEG-ros- b-P(CL_{44}-co-DCL_{10}), mPEG-ros-P(CL_{43}-co-DCL_{22}), and mPEG-ros- b-P(CL_{45}-co-DCL_{33}) were determined to be 3.3 μg/mL, 5.1 μg/mL, and 7.1 μg/mL, respectively. The increase of the DCL content resulted in an increase in the CAC. These results may be due to the fact that the introduction of the dimethyl maleamidic acid groups to the polyester of mPEG-b-PCL decreased the hydrophobicity of polyester chains. It was well-known that the main driving force of forming NPs in water is the hydrophobic interactions of hydrophobic segments. Therefore, the CAC value of mPEG-ros- b-P(CL-co-DCL)was increased with the increase of the number of DCL units. The amphiphilic mPEG-b-P(CL-co-DCL) can self-assemble into NPs with a hydrophobic core (P(CL-co-DCL)) and a hydrophilic corona (mPEG) in water.

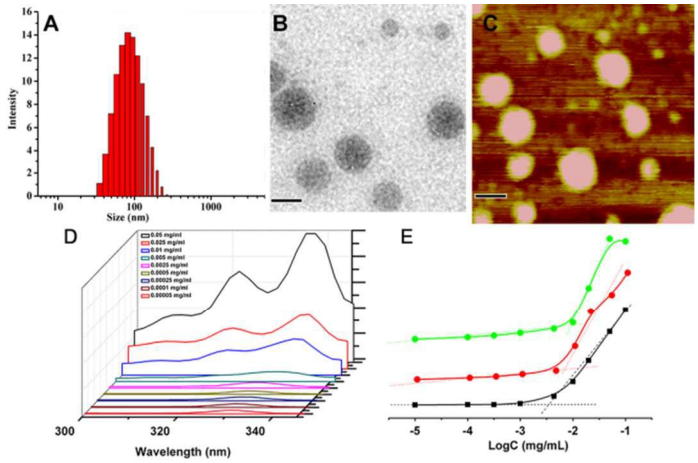

Fig. 2 Size distributions (A), TEM micrograph (B) and AFM (C) micrograph. The scale bar is 100 nm. Fluorescence emission spectra of pyrene in the presence of decreasing concentrations of mPEG-ros-P(CL-co-DCL) (D) and Plot of I337/I333 in the excitation spectrum versus the concentrations of copolymers in water (E).

Table 2. Characteristics of blank and DOX-loaded mPEG-ros-P(CL-co-DCL) NPs.

Copolymers	blank NPs			DOX-loaded NPs			
	Size (nm)[a]	CAC (mg/mL)[b]	PDI [a]	Size (nm)[a]	PDI	DLC (%)[c]	DLE (%)[c]
$mPEG_{113}$-b-PCL_{67}	95 ± 8	1.3× 10-3	0.13	117 ± 9	0.13	3.9±0.2	26±1.3
$mPEG_{113}$-ros-P(CL_{42}-co-DCL_{10})	105 ± 10	3.3×10^{-3}	0.14	90 ± 9	0.14	7.7±0.3	51±2
$mPEG_{113}$-ros-P(CL_{41}-co-DCL_{22})	116 ± 11	5.1×10^{-3}	0.16	101 ± 10	0.15	9.6±0.1	64±0.6
$mPEG_{113}$-ros-P(CL_{43}-co-DCL_{33})	131 ± 13	7.1×10^{-3}	0.15	122 ± 11	0.16	11.6±0.2	77±1.3

[a] Determined using Laser particle size analyzer at 25°C in PBS (10 mM, pH 7.4).
[b] measured by a fluorescence technique with pyrene as a probe.
[c] Feed ration of DOX to polymers was 15 mg/100 mg.

Charge-conversional property of mPEG-ros-P(CL-co-DCL) NPs

The surface charge of mPEG-ros-P(CL-co-DCL) NPs was significantly influenced by environmental pH due to the acid-labile β-carboxylic amides in the polyester moiety acid condition. As shown in **Fig. 3**, in order to evaluate the ability of pH-triggered charge reversal, the effect of pH on ζ-potential of blank and DOX-loaded $mPEG_{113}$-ros-P(CL_{41}-co-DCL_{22}) NPs at physiological environment (pH 7.4) and tumor microenvironment (pH 6.0) was measured. The DOX-loaded NPs and blank NPs' ζ-potentials was negatively charged at pH 7.4 (about -7 mV and -14 mV, respectively). It can be observed that both bland and DOX-loaded $mPEG_{113}$-ros-P(CL_{41}-co-DCL_{22}) NPs at pH 7.4 remained negatively charged even after 12 h. This can be ascribed to the inertness of negatively charged dimethyl maleamidic acid groups at pH 7.4. However, at pH 6.0, the ζ-potential of bland and DOX-loaded $mPEG_{113}$-ros-P(CL_{41}-co-DCL_{22}) NPs changed sharply from negative to high positive in a short time. It only took about 0.4 h for blank NPs and about 1.0 h for DOX-loaded NPs to become positively charged. Compared with blank NPs, DOX-loaded $mPEG_{113}$-ros-P(CL_{41}-co-DCL_{22}) NPs had a slower charge reversal rate at pH 6.0, which may be due to the effect of the loaded DOX. Some studies have confirmed that cationic DOX and carboxyl derivatives can form very stable ionic complexes[56]. In addition, these results indicated the charge reversal process was very fast due to the quick and effective detachment of the acid-labile β-carboxylic amides.

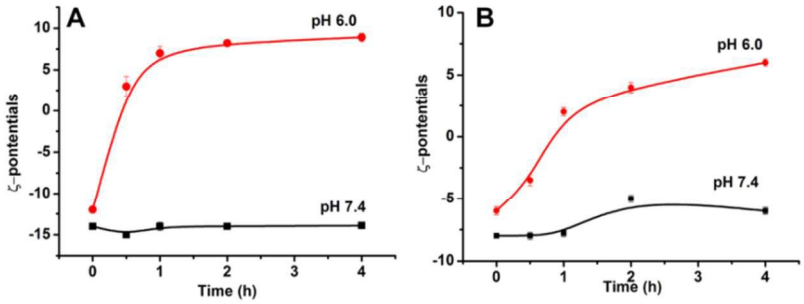

Fig. 3 ζ-potentials changes of blank and DOX loaded mPEG-ros-P(CL-co-DCL) NPs at pH 7.4 (A) and 6.0 (B).

pH and ROS sensitivity of mPEG-ros-P(CL-co-DCL)

The pH and ROS sensitivity of NPs was examined by monitoring the size change of NPs at pH 7.4, 6.0 and 5.4 with or without 10 mM H_2O_2 at 37 °C. The **Fig. S5** shown he ROS responsive mechanism of thioether. As shown in **Fig. S6**, after the 10 mM H_2O_2

treatment, the molecular weight was smaller than that of the untreated mPEG-ros-P(CL-co-DCL) polymer, which was attributed to the cleavage of thiother resulting the degradation of mPEG-ros-P(CL-co-DCL). In view of the potential utility of NPs formulation for pharmaceutical applications, stability is significant for long-term storage, transportation, and scalable processing. As shown in **Table S1**, stability study was carried out by re-dissolving NPs in PBS at 37 ^{o}C for 3 days to assess the size change. The stability of the nanoparticles as drug carriers in PBS containing serum or proteins is also important. As shown in Table S1, the particle size of nanoparticles did not change distinctly in 3 day in PBS containing 10% (v/v) FBS. As shown in **Fig. 4A**, under physiological conditions (pH 7.4) without 10 mM H_2O_2, little size changes of NPs were observed over 24 h. However, at the same condition of pH 7.4 with H_2O_2 (**Fig. 4B**), the increase in size of mPEG-ros-P(CL-co-DCL) NPs from about 100 nm to 200 nm in 4 h was found. The fast aggregation behaviors were ascribed to that the thiother chain linker of mPEG-ros-P(CL-co-DCL) polymers could be easily oxidized by ROS and thus become hydrophilic, triggering hydrolysis of the phenol ester of polymers. The breakage of the phenol ester of backbone leaded to the morphological changes of the nanostructure. Furthermore, the variation of backscattering data (ΔBS), depended on the mean particle size and their volume fraction was used to reflect the ROS sensitivity of NPs as shown in **Fig. 4G** and **H**. The ΔBS profiles remained close to the base line value were observed for the mPEG-ros-P(CL-co-DCL) at pH 7.4 without H_2O_2 during the entire time of analysis. This finding showed that no creaming or sedimentation occurred during the entire time. At the same time, positive or negative ΔBS profiles of the different formulation were not correlated to destabilitzation processes under the sample height of 2 mm and over that 40 mm. The values had been determined by enclosed air in the bottom and/or on the top of the cylindrical glass tube, respectively. Remarkably, as shown by ΔBS profiles in **Fig. 4H**, extreme unstability behavious of mPEG-ros-P(CL-co-DCL) NPs at 10 mM H_2O_2 were observed, reflecting the cleavage of ROS-sensitive thioether bonds. When mPEG-ros-P(CL-co-DCL) NPs were treated in pH 6.0 and pH 5.4 with the absence of 10 mM H_2O_2, significant changes of NPs sizes were observed in **Fig. 4C and E**. The dimethyl maleamidic acid groups, under acidic environments, would be quickly hydrolyzed and changed into cationic primary amines. The change broke the hydrophilic and hydrophobic balance that is critical for micellar stability. As a result, the aggregation of mPEG-b-P(CL-co-DCL) NPs at pH 6.0 and 5.4 was happened. Under mildly acidic (pH 6.0 or 5.4) and 10 mM H_2O_2 conditions, the fastest changes in size of mPEG-ros-P(CL-co-DCL) NPs were also observed in **Fig. 4D and F**. The increase in diameter of NPs after 4 h were seen and a large number of nano-aggregates were found. However, when the NPs suspension was incubated for 24 h, a large number of 13.0 nm particles were detected, indicating that mPEG-ros-P(CL-co-DCL) NPs were inclined to form hydrophilic unimers after PEG shedding.

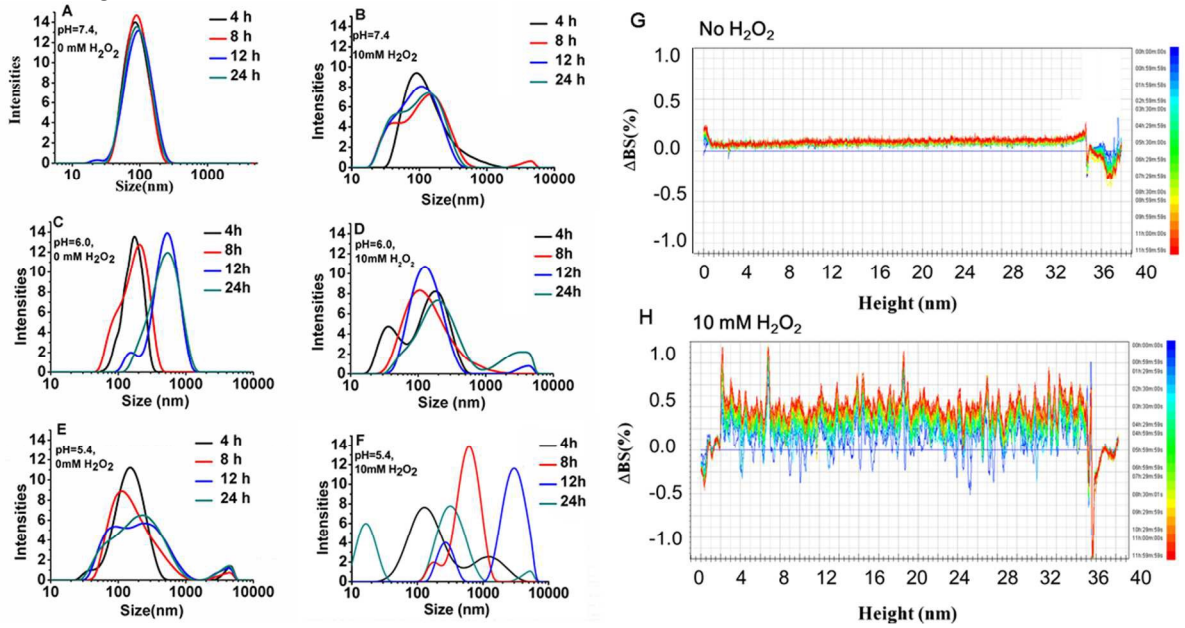

Fig. 4 Time dependence of the size changes of NPs in pH 7.4 (A), 6.5 (C) and 5.0 (E) without 10 mM H_2O_2 and pH 7.4 (B), 6.5 (D) and 5.0 (F) with 10 mM H_2O_2. Variation of backscattering data (△BS) of mPEG-ros-P(CL-co-DCL) NPs at pH 7.4 without 10 mM H_2O_2 (G) and with 10 mM H_2O_2 (H) measured along the height axis of the sample tube. Data from bottom to top are given for different periods of time.

DOX loading and release

DOX as a model chemotherapeutic agent was used to evaluate the loading and releasing properties of mPEG-ros-P(CL-DCL) NPs with ROS-sensitivity. DOX-loaded mPEG-ros-P(CL-co-DCL) NPs were prepared at a polymer concentration of 1 mg/mL. The characteristic of the DOX-loaded NPs, including size, size distribution, loading content and encapsulation efficiency were summarized in **Table 2**. The NPs sizes slightly decreased after loading different amount of DOX. As mentioned above, DOX can interact with carboxyl of DCL units by electrostatic attraction, leading to a more compact structure of micellar core and thus a

smaller size of NPs. All the PDI remained in a narrow range of 0.15-0.19. Compared with mPEG-b-PCL, mPEG-ros-P(CL-co-DCL) NPs showed a much higher drug loading capacity. The drug loading content and encapsulation efficiency of mPEG-b-P(CL-co-DCL) NPs were nearly 3 ~ 4 times higher than that of mPEG-b-PCL NPs. Moreover, the drug loading content and encapsulation efficiency of mPEG-ros-P(CL-co-DCL) NPs increased with increasing the content of DCL units. These phenomena can be due to the electrostatic interaction between DOX and carboxyl. The carboxyl derivatives, such as oleic acid, polyglutamic acid and polymalic acid, have widely been used to enhance the DOX-loading capacity and efficiency. We chose DOX loaded $mPEG_{113}$-ros-$P(CL_{41}$-co-$DCL_{22})$ NPs as a representative sample for next study.

The *in vitro* drug release studies were carried out at pH 7.4 and 6.0 with or without 10 mM H_2O_2. As shown in **Fig. 5A**, the results showed that the release of DOX from NPs was obviously faster at 10 mM H_2O_2 than at physiological condition. For instance only approximately 26 % of DOX was released from DOX loaded NPs within 24 h, indicating that the NPs were relatively stable under physiological condition (pH 7.4). However, the release of DOX was significantly accelerated at 10 mM H_2O_2 with about 62 % of DOX release. As shown in **Fig. 5B**, about 80 % DOX was released in 24 h at pH 6.0. The significant increase in DOX release from NPs in acidic medium can be ascribed to the fact that the pH-induced hydrolysis of the dimethyl maleamidic acid groups resulted in a quick charge reversal, as demonstrated above. Owing to the charge conversion, a repulsive electrostatic force will generate in the DOX loaded NPs, which can greatly accelerate the release rate of the drug. Interestingly, as shown in **Fig. 5C**, under mildly acidic (pH 6.0) and 10 mM H_2O_2 conditions, the release of DOX was further improved to 91 % in 24 h, which might be due to synergistic effect of pH and ROS dual induced disassembly of NPs.

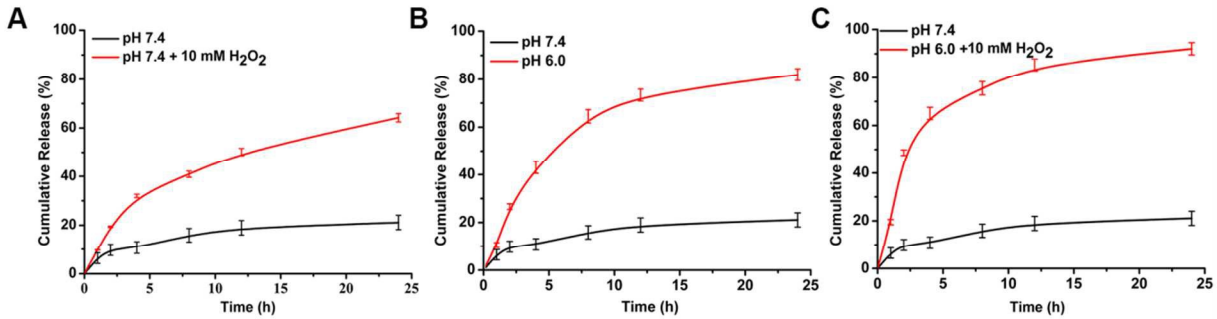

Fig. 5 In vitro release of DOX from DOX loaded NPs at pH 7.4 with 10 mM H_2O_2 (A), pH 6.0 (B) and pH 6.0 with 10 mM H_2O_2 (C).

Intracellular uptake and release

To demonstrate whether mPEG-ros-P(CL-co-DCL) NPs could be efficiently internalized by cancer cells, the cellular uptake behaviors of mPEG-ros-P(CL-co-DCL) NPs was investigated at pH 7.4 and 6.8. We incubated the mPEG-ros-P(CL-co-DCL) NPs with HepG2 cancer cells at each pH for 4 h, and their cellular distribution was evaluated by using confocal laser scanning microscope (CLSM). As shown in **Fig. 6A**, after 4 h incubation, stronger DOX fluorescence appeared both in the cytoplasm and in the nuclei of HepG2 cells for free DOX than the DOX-loaded mPEG-ros-P(CL-co-DCL) NPs. It had been known that DOX molecule is membrane permeable and can be internalized into tumor cells through a passive diffusion mechanism while the DOX-loaded NPs need to be endocytosed. Comparing DOX-loaded mPEG-ros-P(CL-co-DCL) NPs at pH 6.8 and pH 7.4, the former showed higher DOX fluorescence than the latter. Thus DOX-loaded mPEG-ros-P(CL-co-DCL) NPs were remarkably internalized at pH 6.8, which was mostly due to the significantly enhanced cellular internalization of charge-conventional mPEG-ros-P(CL-co-DCL) NPs. Following cellular internalization, another key issue is whether the DOX molecule can be efficiently released from the NPs, triggered by the intact intracellular ROS. To demonstrate this, HepG2 were treated with phorobol 12-myristate 13-acetate (PMA) to accelerate the generation of ROS. The treatment of HepG2 cells with PMA (200 nM) increased the intracellular ROS level, compared to cells without PMA treatment. Then we incubated HepG2 and PMA treated HepG2 cells with DOX-loaded mPEG-ros-P(CL-co-DCL) NPs. As shown in **Fig. 6B**, after 4 h incubation, compared with the PMA treated HepG2 cells, the intracellular DOX fluorescence was stronger than untreated HepG2. The enhanced fluorescence intensity in the PMA pretreated HepG2 cells should be due to the rapid intracellular DOX release from the DOX-loaded mPEG-ros-P(CL-co-DCL). The enhanced cellular internalization of charge-conventional mPEG-ros-P(CL-co-DCL) NPs can be also confirmed by flow cytometric analyses of the HepG2 cells incubated with free DOX, DOX-loaded mPEG-ros-P(CL-co-DCL) NPs at pH 7.4 and 6.8 as shown in **Fig. 6C**. The ROS responsive nature of DOX laoded mPEG-ros-P(CL-co-DCL) NPs was also studied by flow cytometric analyses of the PMA treated HepG2 cells and untreated cells as shown in **Fig. 6D.** In order to imitate the In vivo status of tumor more accurately, the tumor spheroid was used to evaluate the stability of charge-conventional mPEG-ros-P(CL-co-DCL) NPs. As shown in **Fig. 6E,** the stronger fluorescent intensity of tumor spheroid incubated in pH 6.8 was observed than in pH 7.4, suggesting that the enhanced cellular internalization of charge-conventional mPEG-ros-P(CL-co-DCL) NPs in extracellular environment.

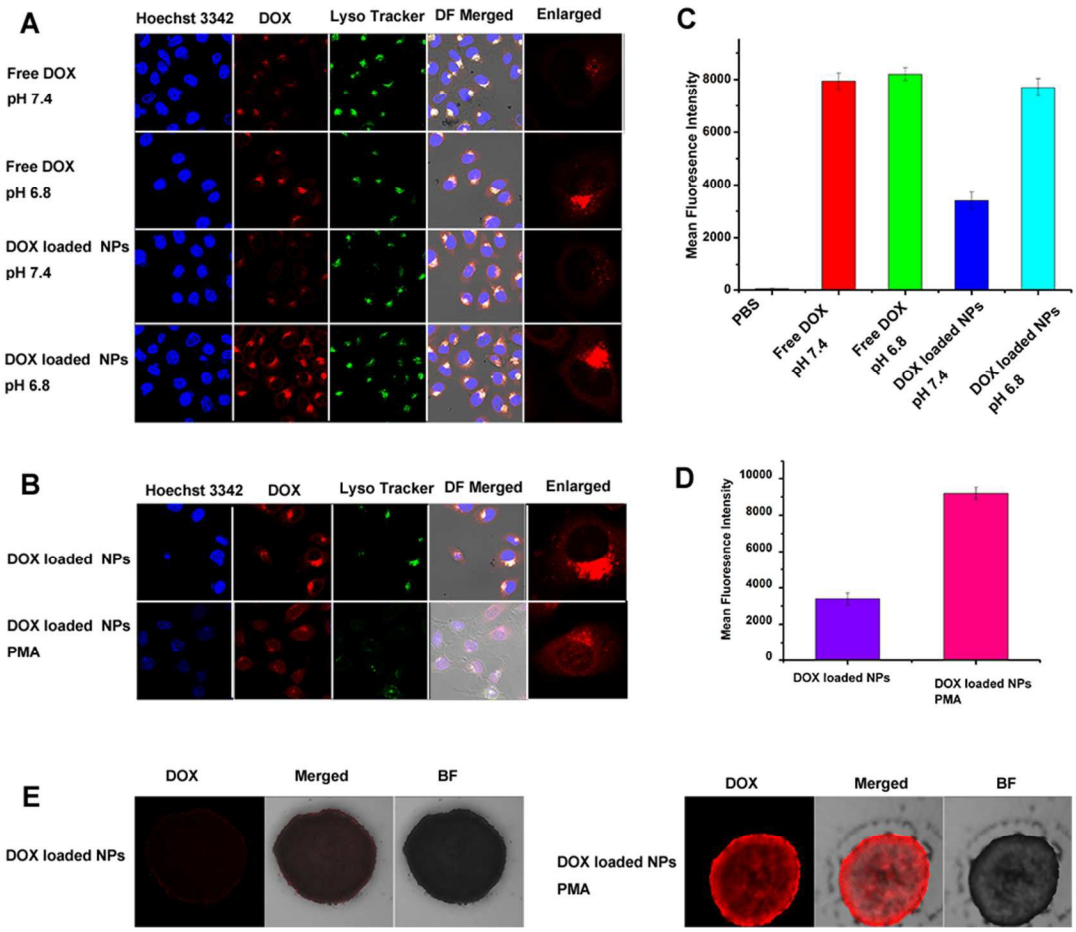

Fig. 6 (A) Representative CLSM images of HepG2 cells incubated with DOX-loaded mPEG-ros-P(CL-co-DCL) NPs and free DOX (10 μg/mL) at pH 7.4 and 6.8. (B) Flow cytometric comparison of cell uptake of NPs at different pH (10 μg/mL). (C) Representative CLSM images of HepG2 cells incubated with DOX-loaded mPEG-ros-P(CL-co-DCL) NPs and free DOX (10 μg/mL) with or without PMA (200 nM). (D) Flow cytometric comparison of cell uptake of NPs with or without PMA. (E) Fluorescence distribution of HepG2 tumor spheroids after incubated with mPEG-ros-P(CL-co-DCL) (at pH 7.4 or 6.8), the concentration of DOX was 10 ug/mL and bar represents 200 mm.

Cell Viability Assays

The cytotoxicity of NPs was investigated in HepG2 cells (tumor cells) and L02 cells (normal cells) by MTT assays. The results showed that mPEG-ros-P(CL-co-DCL) NPs were practically nontoxic to HepG2 and L02 cells (cell viabilities: 80-90 %), indicating that these NPs possess excellent biocompatibility as shown in **Fig. 7A**. The cytotoxicity of DOX loaded mPEG-ros-P(CL-co-DCL) was studied in HepG2 cells. To demonstrate the effect of ROS responsive ability of mPEG-ros-P(CL-co-DCL) NPs in cells, the viability of HepG2 cells treat with or without PMA were investigated. **Fig. 7B** showed that DOX loaded mPEG-ros-P(CL-co-DCL) NPs caused significant cell death (half maximal inhibitory concentration (IC50): 2.28 μg/mL) treated with PMA which was comparable to that of without PMA group (IC50: 5.66 μg/mL). This may be due to that the high ROS concentration of HepG2 cells treat with PMA caused cleavage of ROS-sensitive bonds in NPs. This demonstrated that following cellular internalization, DOX molecules can be efficiently released from the NPs, triggered by intracellular ROS. Besides, the DOX-loaded mPEG-ros-P(CL-co-DCL) NPs showed a lower cytotoxicity than that of free DOX (IC50 0.66 μg/mL). The lower cytotoxicity of DOX loaded mPEG-ros-P(CL-co-DCL) NPs may be due to the incomplete drug release from NPs and delayed nuclear uptake. Remindfully, the intracellular uptake results in **Fig. 6** showed that the charge-reversal mPEG-ros-P(CL-co-DCL) NPs could efficiently cross the cell membrane and deliver DOX into the nuclei, so, it is supposed that the mPEG-ros-P(CL-co-DCL) NPs could simultaneously enhance cellular uptake and promote acid-triggered intracellular drug release. Finally, to demonstrate the potential of ROS-responsive mPEG-ros-P(CL-co-DCL) NPs as a novel approach for cancer therapy, the capability of DOX loaded mPEG-ros-P(CL-co-DCL) NPs to selectively inhibit tumor cell proliferation was studied by testing noncancerous and cancer cells. As shown in **Fig. 7C,** the cytotoxicity of DOX loaded mPEG-ros-P(CL-co-DCL) NPs against the noncancerous L02 cells treated with or without PMA was measured by MTT assay. The *in vitro* IC50 values were 5.17 μg/mL for DOX-loaded mPEG-ros-P(CL-co-DCL) NPs treated with PMA. However, the noncancerous L02 cells without PMA treatment retained over 60 % viability suggesting that DOX loaded

mPEG-ros-P(CL-co-DCL) NPs is highly selective in inhibiting tumor cell proliferation. These results were in agreement with the previously reports.[57]

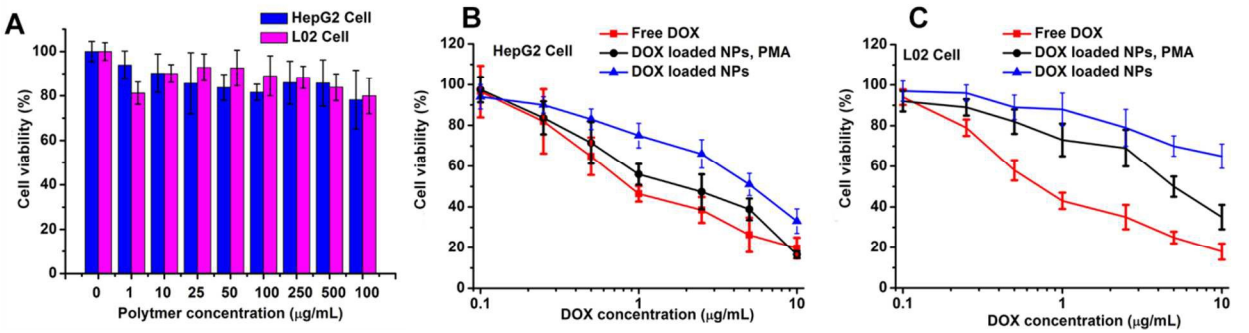

Fig. 7 (A) Viability of HepG2 and L02 cells after incubation for 24 h with mPEG-ros-P(CL-co-DCL) NPs at various specified concentrations. (B) Viability of HepG2 cells after being incubated with free DOX, DOX loaded mPEG-ros-P(CL-co-DCL) NPs and DOX loaded NPs with PMA for 24 h. (C) Viability of L02 cell after being incubated with free DOX, DOX loaded mPEG-ros-P(CL-co-DCL) NPs and DOX loaded NPs with PMA for 24 h.

Conclusion

In this work, we firstly reported a series of multifunctional PEG-b-PCL copolymers bearing acid-labile β-carboxylic amides-modified PCL chain with the ability of acid-triggered charged-reversal from negative to positive to enhance cell uptake and ROS sensitive thioether linker between PEG and PCL for targeted intracellular DOX release. Moreover, due to the electrostatic interaction between DOX and carboxyl, the mPEG-ros-P(CL-co-DCL) NPs exhibited a very high drug loading capacity and loading efficiency. The dimethyl maleamidic acid groups on the polyester segment of mPEG-ros-P(CL-co-DCL) can be hydrolyzed under acidic environment and resulted in a quick charge reversal, which had great influence on the drug release profiles, cell internalization process and endo-lysosomal escape. The ROS-response property is also favorable for targeted drug delivery. Intracellular uptake and *in vitro* cytotoxicity studies confirmed that the charge-conversional DOX-loaded NPs exhibited the remarkably enhanced cellular uptake by the combination of electrostatic absorptive endocytosis and antitumor efficiency at the tumor intracellular ROS. The capability of DOX loaded mPEG-ros-P(CL-co-DCL) NPs to selectively inhibit tumor cell proliferation was proved by testing noncancerous and cancer cells. We convinced that the charge-reversible and ROS-sensitive PEG-b-PCL was demonstrated to be effective in killing tumor cells, which provided a versatile approach for efficient cancer therapy.

Acknowledgements

This research was financially supported by National Natural Science Foundation of China (31470963，81371667).

Notes and references

The authors declare no competing financial interest

1 G. S. Kwon and K. Kataoka, *Adv. Drug. Deliver. Rev*, 1995, **16**, 295-309.
2 J. Sankaranarayanan, E. A. Mahmoud, G. Kim, J. M. Morachis and A. Almutairi, *Acs Nano*, 2010, **4**, 5930-5936.
3 H. Maeda, J. Wu, T. Sawa, Y. Matsumura and K. Hori, *J. Control. Release*, 2000, **65**, 271-284.
4 C.-C. Song, R. Ji, F.-S. Du and Z.-C. Li, *Macromolecules*, 2013, **46**, 8416-8425.
5 Y. Y. Kim, B. Hwang, S. Song, B. J. Ree, Y. Kim, S. Y. Cho, K. Heo, Y. K. Kwon and M. Ree, *Nanoscale*, 2015, **7**, 14774-14785.
6 H. Wei, R.-X. Zhuo and X.-Z. Zhang, *Prog. Polym. Sci*, 2013, **38**, 503-535.
7 Y. Lu, J. Yang and E. Sega, *The AAPS journal*, 2006, **8**, 466-478.
8 S. Lv, W. Song, Z. Tang, M. Li, H. Yu, H. Hong and X. Chen, *Mol. Pharmaceut*, 2014, **11**, 1562-1574.
9 K. Park, S. Lee, E. Kang, K. Kim, K. Choi and I. C. Kwon, *Adv. Funct. Mater*, 2009, **19**, 1553-1566.
10 B. Yu, C. Tang and C. Yin, *Biomaterials*, 2014, **35**, 6369-6378.
11 S. Xie, Y. Tao, Y. Pan, W. Qu, G. Cheng, L. Huang, D. Chen, X. Wang, Z. Liu and Z. Yuan, *J. Control. Release*, 2014, **187**, 101-117.
12 L. Wang, Y. Yuan, S. Lin, D. Cheng, X. Wang, Q. Jiang and X. Shuai, *Polym. Chem*, 2014, **5**, 4542-4552.
13 J. Li, Y. Han, Q. Chen, H. Shi, S. ur Rehman, M. Siddiq, Z. Ge and S. Liu, *J. Mater. Chem. B*, 2014, **2**, 1813-1824.
14 S. Baek, R. K. Singh, D. Khanal, K. D. Patel, E.-J. Lee, K. W. Leong, W. Chrzanowski and H.-W. Kim, *Nanoscale*, 2015, **7**, 14191-14216.
15 F. Chen, J. Zhang, L. Wang, Y. Wang and M. Chen, *Nanoscale*, 2015, **7**, 15763-15779.
16 S. Ganta, H. Devalapally, A. Shahiwala and M. Amiji, *J. Control. Release*, 2008, **126**, 187-204.
17 E. S. Gil and S. M. Hudson, *Prog. Polym Sci*, 2004, **29**, 1173-1222.
18 S. Pal, S. G. Roy and P. De, *Polym. Chem*, 2014, **5**, 1275-1284.
19 Y. Du, W. Chen, M. Zheng, F. Meng and Z. Zhong, *Biomaterials*, 2012, **33**, 7291-7299.

20 J. Wang, X. Sun, W. Mao, W. Sun, J. Tang, M. Sui, Y. Shen and Z. Gu, *Adv. Materials*, 2013, **25**, 3670-3676.
21 H.-L. Pu, W.-L. Chiang, B. Maiti, Z.-X. Liao, Y.-C. Ho, M. S. Shim, E.-Y. Chuang, Y. Xia and H.-W. Sung, *Acs Nano*, 2014,**8**:1213-21.
22 Y. Yuan, J. Liu and B. Liu, *Angew. Chem. Int. Edit. 2014,**126**,7291-7296*
23 Y. Wang, M. S. Shim, N. S. Levinson, H.-W. Sung and Y. Xia, *Adv. Funct. Mater*, 2014, **24**, 4206-4220.
24 A. Napoli, M. Valentini, N. Tirelli, M. Müller and J. A. Hubbell, *Nat. Mater*, 2004, **3**, 183-189.
25 S. Chai, K. K. To and G. Lin, *Chin. Med*, 2010, **5**, 26.
26 J. Duan, H. M. Mansour, Y. Zhang, X. Deng, Y. Chen, J. Wang, Y. Pan and J. Zhao, *Int. J. Pharmaceut*, 2012, **426**, 193-201.
27 J. Fang, T. Seki and H. Maeda, *Adv. Drug. Deliver. Rev*, 2009, **61**, 290-302.
28 Y. Gao, Y. Chen, X. Ji, X. He, Q. Yin, Z. Zhang, J. Shi and Y. Li, *Acs Nano*, 2011, **5**, 9788-9798.
29 S. Lv, W. Song, Z. Tang, M. Li, H. Yu, H. Hong and X. Chen, *Mol. Pharmaceut*, 2014, **35**, 3851-3864.
30 J. B. Schlenoff, *Langmuir*, 2014,**11**,1562-74..
31 Z. Wang, G. Ma, J. Zhang, W. Lin, F. Ji, M. T. Bernards and S. Chen, *Langmuir*, 2014, **19**,3580-3589.
32 Z. Zhou, Y. Shen, J. Tang, M. Fan, E. A. Van Kirk, W. J. Murdoch and M. Radosz, *Adv. Funct. Mater*, 2009, **19**, 3580-3589.
33 G. Su, H. Zhou, Q. Mu, Y. Zhang, L. Li, P. Jiao, G. Jiang and B. Yan, *The J. Physic. Chem. C*, 2012, **116**, 4993-4998.
34 Y. Huang, Z. Tang, X. Zhang, H. Yu, H. Sun, X. Pang and X. Chen, *Biomacromolecules*, 2013, **14**, 2023-2032.
35 J. Cao, X. Xie, A. Lu, B. He, Y. Chen, Z. Gu and X. Luo, *Biomaterials*, 2014, **35**, 4517-4524.
36 K. P. García, K. Zarschler, L. Barbaro, J. A. Barreto, W. O'Malley, L. Spiccia, H. Stephan and B. Graham, *Small*, 2014, **10**, 516-529.
37 C. Gunawan, M. Lim, C. P. Marquis and R. Amal, *J. Mater. Chem. B*, 2014, **2**, 2060-2083.
38 M. R. K. Ali, S. R. Panikkanvalappil and M. A. El-Sayed, *J. Am Chem Soc*, 2014, **136**,4464-4467.
39 L. Nuhn, S. Gietzen, K. Mohr, K. Fischer, K. Toh, K. Miyata, Y. Matsumoto, K. Kataoka, M. Schmidt and R. Zentel, *Biomacromolecules*, 2014, **15**, 1526-1533.
40 S.-H. Hu, R.-H. Fang, Y.-W. Chen, B.-J. Liao, I. W. Chen and S.-Y. Chen, *Adv. Funct. Mater,* 2014, **24**,4144-4155.
41 L. Li, Q. Yang, Z. Zhou, J. Zhong and Y. Huang, *Biomaterials*, 2014, **35**, 5171-5187.
42 J. Hu, S. Miura, K. Na and Y. H. Bae, *J. Control. Release*, 2013, **172**, 69-76.
43 Y.-H. Chien, Y.-L. Chou, S.-W. Wang, S.-T. Hung, M.-C. Liau, Y.-J. Chao, C.-H. Su and C.-S. Yeh, *Acs Nano*, 2013, **7**,8516-8528
44 Y. Lee, T. Ishii, H. Cabral, H. J. Kim, J. H. Seo, N. Nishiyama, H. Oshima, K. Osada and K. Kataoka, *Angew. Chem. Int. Edit*, 2009, **121**, 5413-5416.
45 K. Miyata, N. Nishiyama and K. Kataoka, *Chem. Soc. Revs*, 2012, **41**, 2562-2574.
46 K. Itaka, K. Yamauchi, A. Harada, K. Nakamura, H. Kawaguchi and K. Kataoka, *Biomaterials*, 2003, **24**, 4495-4506.
47 N. Nishiyama, A. Iriyama, W.-D. Jang, K. Miyata, K. Itaka, Y. Inoue, H. Takahashi, Y. Yanagi, Y. Tamaki and H. Koyama, *Nat. Mater*, 2005, **4**, 934-941.
48 J. Z. Du, T. M. Sun, W. J. Song, J. Wu and J. Wang, *Angew. Chem. Int. Edit*, 2010, **122**, 3703-3708.
49 H. Deng, J. Liu, X. Zhao, Y. Zhang, J. Liu, S. Xu, L. Deng, A. Dong and J. Zhang, *Biomacromolecules*, 2014, **15**, 4281-4292.
50 D. Ling, M. J. Hackett and T. Hyeon, *Nano Today*, 2014, **9**, 457-477.
51 E. Fleige, M. A. Quadir and R. Haag, *Adv. Drug Deliver. Rev*, 2012, **64**, 866-884.
52 J. Zhuang, M. R. Gordon, J. Ventura, L. Li and S. Thayumanavan, *Chem. Soc. Rev*, 2013, **42**, 7421-7435.
53 J. Wang, X. Sun, W. Mao, W. Sun, J. Tang, M. Sui, Y. Shen and Z. Gu, *Adv. Mater*, 2013, **25**, 3670-3676.
54 T. Rossow, J. A. Heyman, A. J. Ehrlicher, A. Langhoff, D. A. Weitz, R. Haag and S. Seiffert, *J. Am. Chem. Soc*, 2012, **134**, 4983-4989.
55 X. Z. Shu, Y. Liu, F. S. Palumbo, Y. Luo and G. D. Prestwich, Biomaterials, 2004, **25**, 1339-1348.
56 A. Jimenez-Kairuz, D. Allemandi and R. Manzo, *Int. J. Pharmaceut*, 2004, **269**, 149-156.
57 M. Wang, S. Sun, C. I. Neufeld, B. Perez-Ramirez and Q. Xu, *Angew. Chem. Int. Edit*, 2014, **53**, 13444-13448.

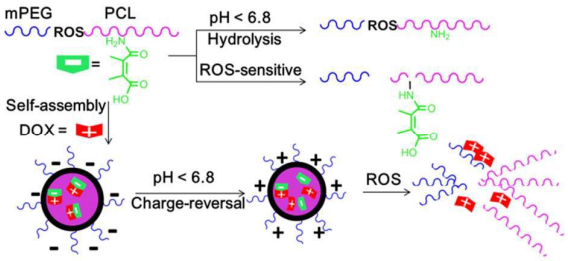

The charge-conversional behavior and ROS-sensitivity of mPEG-ros-P(CL-co-DCL) NPs for active loading and triggered release of DOX